Colloids and Surfaces B: Biointerfaces 83 (2011) 16–22

Contents lists available at ScienceDirect

Colloids and Surfaces B: Biointerfaces

journal homepage: www.elsevier.com/locate/colsurfb

Synthesis of silver nanoparticles in an aqueous suspension of graphene oxide sheets and its antimicrobial activity

Manash R. Das[a,*], Rupak K. Sarma[b], Ratul Saikia[b], Vinayak S. Kale[c], Manjusha V. Shelke[c], Pinaki Sengupta[a]

[a] Materials Science Division, North East Institute of Science & Technology, CSIR, Jorhat 785006, Assam, India
[b] Biotechnology Division, North East Institute of Science & Technology, CSIR, Jorhat 785006, Assam, India
[c] Materials Chemistry Division, National Chemical Laboratory, CSIR, Dr. Homi Bhabha Road, Pune 411008, India

ARTICLE INFO

Article history:
Received 10 July 2010
Received in revised form 15 October 2010
Accepted 19 October 2010
Available online 30 October 2010

Keywords:
Graphene oxide
Silver nanoparticle
Pseudomonous aeruginosa
Escherichia coli
Antimicrobial activity

ABSTRACT

A solution-based approach to the synthesis of silver (Ag) nanoparticles by chemical reduction of $AgNO_3$ in a graphene oxide (GrO) suspension is demonstrated. X-ray diffraction and transmission electron microscopy indicate that the Ag nanoparticles, of size range 5–25 nm, were decorated on the GrO sheets. The size and shape of the Ag nanoparticles are dependent on the concentration of the $AgNO_3$ solution. Antimicrobial activity of such hybrids materials is investigated against the Gram negative bacteria *Escherichia coli* and *Pseudomonous aeruginosa*. The bacterial growth kinetics was monitored in nutrient broth supplemented with the Ag nanoparticle–GrO suspension at different conditions. It was observed that *P. aeruginosa* is comparatively more sensitive to the Ag nanoparticle–GrO suspension.

1. Introduction

Graphene, a single layer of carbon atoms closely packed into honeycomb two-dimensional (2D) lattice, has attracted enormous attention recently [1,2]. Its sp^2 hybrid carbon network as well as extraordinary electronic, thermal and mechanical properties are interesting for wide range of applications [3–6]. Graphite oxide (GO) is a basic material for the preparation of individual graphene sheets in bulk quantity. Its large surface area, oxygen containing surface functionalities such as hydroxyl, carboxylic, carbonyl, epoxide groups and high water solubility are promising for many applications [7,8]. For instance, suspension based on functionalized sheets of graphene or graphene oxide (GrO) provides a convenient route to keep sheets exfoliated and available for ion or nanoparticle intercalation. Metallic nanoparticles play an important role in wide number of applications such as surface-enhanced Raman scattering (SERS), display devices, catalysis, microelctronics, light emitting diodes, photovoltaic cells and also in medical or biological applications [9,10]. Moreover, nanoparticles show changes in its electronic, optical and catalytic properties depending on the method of synthesis [11]. Insertion of the nanoparticles on the graphene based matrix is an important study for the exploration of their properties and applications. Nanoparticles such as TiO_2, Co_3O_4, Pd, Pt, Ag and Au have been achieved using GrO or reduced GrO as substrate [12–23]. Au nanoparticles are synthesized using chemical reduction of $HAuCl_4$ with $NaBH_4$ in graphene octadecylamine suspension [18]. Composites of GrO sheets decorated with magnetic nanoparticles such as iron oxide are developed recently [24]. Multicomponent catalyst systems are developed by anchoring metal and semiconductor nanoparticles at separate sites on reduced GrO substrates. As evident from the literature the functionalization of metal nanoparticles on the graphene based surfaces produces new hybrid materials which have potential importance in the areas such as optics, electronics, catalysis and sensors [7]. The biological studies of graphene and its composite materials are relatively limited. However, recent attention has been drawn towards the antimicrobial activity of graphene and its composites materials [23,25,26]. Shen et al. recently reported the Ag-chemically converted graphene (CCG) nanocomposite that shows very good antibacterial activity against *Colibacillus*, *S. aureus* and *C. albicans* [23]. Ag-CCG reported to show the high disinfection ability and completely destroys the bacterial cultures.

Silver (Ag) is an attractive material for its distinctive properties, such as good conductivity, chemical stability, catalytic activity and antimicrobial activity [27]. Ag nanoparticles are used in antimicrobial applications since the antimicrobial effect of Ag ions is well known [28–31]. Ag nanoparticles showed cytoprotective activity towards HIV-1 infected cells [32]. It is being used in the med-

* Corresponding author. Tel.: +91 376 2370081; fax: +91 376 2370011.
E-mail address: mnshrdas@yahoo.com (M.R. Das).

0927-7765/$ – see front matter © 2010 Elsevier B.V. All rights reserved.
doi:10.1016/j.colsurfb.2010.10.033

ical field as well as in water and air filtration [33–35]. Hybrid materials of Ag nanoparticles with amphiphilic hyperbranched macromolecules are synthesized for use in surface coatings because of its antibacterial activity [36]. The surfaces coated with Ag nanoparticles embedded paint based on vegetable oil showed excellent antimicrobial properties [37]. The water related diseases like diarrhea and dehydration can be reduced by improving the microbial quality of the drinking water. The bactericidal activity can be reduced by the use of the Ag deposited carbon filters [38–40]. Bioaerosol are the airborne particles which cause chronic diseases. These bioaerosol develop in the ventilating, heating and air-conditioning system in humid atmosphere. The use of Ag coated activated carbon filter (ACF) effectively removes bioaerosols [41]. There are several commercial products for wound treatment that contain Ag as an antimicrobial agent. Nanocrystalline Ag in wound dressings is used to treat ulcers, and Ag sulfadiazine is used in pastes or creams for treating burn wounds [42].

A desire to exploit the unique biomedical properties of Ag nanoparticles led us to synthesis Ag nanoparticles on GrO matrix. We believe that the hybrid material of Ag nanoparticles where a layered material like GrO is used as matrix can induce binding capability that usually lacks in Ag nanoparticles alone and thus enhance its antimicrobial activity. So far Ag nanoparticles are synthesized on GrO substrate in the presence of KOH without any reducing agent [15]. The hydroxyl groups present in the hexagonal basal plane play a crucial role for the reduction of the Ag salt. The phenols undergo deprotonation in the presence of KOH and produce phenolate anions. These phenolate anions take part in electrophilic substitution by transferring electron to the Ag ion to form the metallic Ag. Zhou et al. reported the one step *in situ* synthesis of Ag nanoparticles on GrO or reduced GrO substrate without using any surfactant or reducing agent [12]. GrO substrate was prepared by adsorption of GrO on 3-aminopropyltriethoxysilane (APTES) modified SiO_x substrate. This substrate was immersed in an aqueous solution of $AgNO_3$ under N_2 protection and heating at 75 °C. The electron in the negatively charge GrO substrate is participated for the reduction of Ag ion to get the metallic Ag. Recently Shen et al. reported the solution based synthesis of Ag nanoparticles in CCG suspension with mixed reducing agent, ethylene glycol and $NaBH_4$ [23]. They have investigated the SERS activity and the antibacterial activity of the synthesized Ag-CCG composite. Herein we report solution phase synthesis of Ag nanoparticles by reduction of $AgNO_3$ on GrO matrix with $NaBH_4$ as a reducing agent at normal atmospheric conditions and its *in situ* characterization. The antimicrobial activity of Ag nanoparticles on GrO is also studied in details against the Gram negative bacteria *Escherichia coli* (*E. coli*) and *Pseudomonous aeruginosa* (*P. aeruginosa*).

2. Materials and methods

2.1. Materials

Graphite powder (<20 micron) was purchased from Sigma-Aldrich, Germany and used as-received. $AgNO_3$ (99.8%, Qualigens, India), $NaBH_4$ (>99%, S.D. Fine, India), hydrochloric acid (AR grade, Qualigens, India), H_2O_2 (30% (w/v), Qualigens, India), $KMnO_4$ (>99%, NICE-Chemical, India), nutrient broth (g/l, peptone 5 g, beef extract 3 g, sodium chloride 5 g; pH 7; HiMedia, Mumbai, India) were used as-received and without any further purification.

2.2. Preparation of GrO

GO was prepared from powder graphite adopting Hummer and Offeman method [43]. Generally, 1 g of graphite powder was added to 23 mL of concentrated H_2SO_4 in an ice bath. $KMnO_4$ (3 g) was then added slowly with stirring and cooling to keep the temperature of the reaction mixture below 20 °C. The temperature of the reaction mixture was increased and maintained at 35 °C for 30 min. When 46 mL of deionized water was added slowly to this mixture temperature was increased to 98 °C. After 15 minutes 140 mL of deionized water was added followed by 10 mL of 30% H_2O_2 solution. The solid product was separated by centrifugation. It was washed repeatedly with 5% HCl solution until the sulfate ions are removed and then washed with distilled water repeatedly until it becomes free of chloride ions. The product was then filtered and washed 3–4 times with acetone to make it moisture free and the residue thus obtained was dried in an air-oven at 65 °C overnight. The GO was suspended in water and exfoliated through ultrasonication for 3 h. A homogeneous reddish brown solution of GrO nanosheets was obtained. This GrO–water suspension was used as a matrix for the preparation of the Ag nanoparticles.

2.3. Preparation of Ag nanoparticles on GrO

Ag nanoparticles were prepared by reducing $AgNO_3$ with $NaBH_4$ in presence of GrO suspension. In the typical procedure, 10 mL of homogeneous suspension of GrO was mixed with the desired amount of aqueous $AgNO_3$ solution (1×10^{-3} mol dm^{-3}, 2×10^{-3} mol dm^{-3}, 4×10^{-3} mol dm^{-3} and 8×10^{-3} mol dm^{-3} $AgNO_3$). The reaction mixture was stirred for 30 min at room temperature before addition of the reducing agent. 1 mL of 0.01 mol dm^{-3} freshly prepared solution of $NaBH_4$ was added slowly to the reaction mixture of $AgNO_3$–GrO suspension under vigorous stirring. The color of the reaction mixture turns into dark brown to grey depending on the concentration of the $AgNO_3$. The reaction mixture was stirred for another 5 h for the complete reduction at room temperature.

2.4. Antibacterial activity of Ag nanoparticles

The antibacterial activity of Ag nanoparticles was studied against Gram negative bacterial strains, *E. coli* and *P. aeruginosa*. The bacterial strains were grown in nutrient broth (NB) at 30 °C with continuous shaking at 200 rpm for 24 h. The bactericidal effect was studied in nutrient agar medium by using 60 μL of suspension of Ag nanoparticles synthesized with different concentrations of $AgNO_3$ (1×10^{-3} mol dm^{-3}, 2×10^{-3} mol dm^{-3}, 4×10^{-3} mol dm^{-3} and 8×10^{-3} mol dm^{-3} $AgNO_3$) and 60 μL of bacterial cultures (approx. 10^8 Colony-forming unit [CFU]) by agar well diffusion assay [44]. The zone of inhibition was recorded after 24 h incubation at 30 °C.

2.5. Bacterial growth kinetics

The bacterial growth kinetics was studied by colorimetric method [30]. 5 μL of bacterial suspension was inoculated individually in 10 mL of NB supplemented with 5 μL of different doses of Ag nanoparticles, it was incubated at 30 ± 1 °C temperature with continuous agitation at 200 rpm. Growth kinetics was determined by measuring optical density at 660 nm at every 1 h interval from the time of inoculation with 3 replications.

2.6. Characterization

Preliminary characterization of formation of Ag nanoparticles was made by UV–Visible spectroscopy. UV–Visible spectra were recorded in the range between 200 and 800 nm using Specord 200 (Analytik Zena, Germany). The Ag nanoparticle–GrO suspension was diluted 10 times to record the UV–Visible spectra.

X-ray diffraction (XRD) measurement was carried out by Rigaku X-ray diffractometer (Model: ULTIMA IV, Rigaku, Japan) with Cu Kα

X-ray source (λ = 1.54056 Å) at a generator voltage 40 kV, a generator current 40 mA with the scanning rate 2° min^{-1}.

The high resolution transmission electron microscopy (HRTEM) images were taken by a TECNAI-T 30 model instrument operated at an accelerating voltage of 300 kV. Samples for HRTEM imaging were prepared by placing a drop of the solution sample in deionised water onto a carbon-coated Cu grid (3 nm thick, deposited on a commercial copper grid for electron microscope), dried in air and loaded into the electron microscopic chamber.

3. Results and discussion

The preliminary investigations of the formation of the Ag nanoparticles on GrO–water suspension are carried out by UV–Visible spectroscopy. The UV–Visible spectra of the Ag nanoparticles on GrO–water suspension using different concentrations of aqueous $AgNO_3$ solution is shown in Fig. 1. The appearance of characteristic surface plasmon band at 400 nm indicates the formation of Ag nanoparticles on GrO–water suspension [45]. The surface plasmon band of the Ag nanoparticles is appeared at 400 nm when 1×10^{-3} mol dm^{-3} and 2×10^{-3} mol dm^{-3} of $AgNO_3$ solutions are used to prepare Ag nanoparticles. However, the absorption band is shifted to longer wavelength in case of higher concentrations of $AgNO_3$ (407 nm for 4×10^{-3} mol dm^{-3} and 417 nm for 8×10^{-3} mol dm^{-3}). The shifting of the absorption peak towards longer wavelength for the higher concentration of $AgNO_3$ indicates the formation of larger Ag nanoparticles, with different shapes and sizes [46]. This is also supported by transmission electron microscope (TEM) analysis. A hump at 350 nm in case of synthesized Ag nanoparticles using 4×10^{-3} mol dm^{-3} and 8×10^{-3} mol dm^{-3} of $AgNO_3$ implies polydispersity of the size and shape of the nanoparticles [47]. Usually surface plasmon band shifts depending on the particle size, shape, chemical surrounding, adsorbed species on the surface and dielectric constant [48,49].

The formation of the Ag nanoparticles is further confirmed by XRD analysis. The XRD patterns are shown in Fig. 2. The prominent peak at 2θ values of about 38.1°, 44.3°, 64.5° and 77.5° are assigned to the (1 1 1), (2 0 0), (2 2 0) and (3 1 1) crystallographic planes of face-centered cubic (fcc) Ag nanoparticles, respectively [JCPDS card No. 07-0783]. The corresponding *d*-spacing values of the Ag nanoparticles are 2.36, 2.04, 1.44 and 1.23 Å, respectively. It is also observed that the *d*-spacing value of the synthesized Ag nanoparticles using different concentration of the $AgNO_3$ remains almost constant for the each crystallographic plane. XRD pattern (Fig. 2) show that the peaks for (1 1 1) and (2 0 0) planes of the Ag nanoparticles are prominent for all the $AgNO_3$ concentration range used. Whereas the peaks for other two planes (2 2 0) and (3 1 1) of the Ag nanoparticles could not be detected in low concentration range (1×10^{-3} mol dm^{-3} and 2×10^{-3} mol dm^{-3}). On the other hand all four crystallographic planes (1 1 1), (2 0 0), (2 2 0) and (3 1 1) are distinct for the nanoparticles synthesized using $AgNO_3$ concentration of 4×10^{-3} mol dm^{-3} and 8×10^{-3} mol dm^{-3}. The high intense diffraction peak observed at 38.1°, corresponding to the crystalline Ag, confirms that the nanoparticles are composed of pure crystalline Ag. The crystallite size of the Ag nanoparticle is calculated by Sherrer equation using PDXL software. The full width half maxima (FWHM), crystallite size and crystalline lattice constant '*a*' of the synthesized Ag nanoparticles using different concentrations of $AgNO_3$ are presented in Table 1. The calculated lattice constant value '*a*' (4.086 ± 0.003) is found to be in very good agreement with the literature value (4.0862) (JCPDS card No. 04-0783).

XRD (inset Fig. 2) also shows that the regular layered structure of GO is completely destroyed at the concentration of 8×10^{-3} mol dm^{-3} $AgNO_3$ solution. The insertion of Ag nanoparticles on GrO sheets prevents restacking of the layered structure of GO [22]. Due to the formation of larger particle of Ag nanoparticles on GrO matrix, the prominent peak of GO at 10.14° (2θ) disappeared when higher concentration of 8×10^{-3} mol dm^{-3} $AgNO_3$ solution

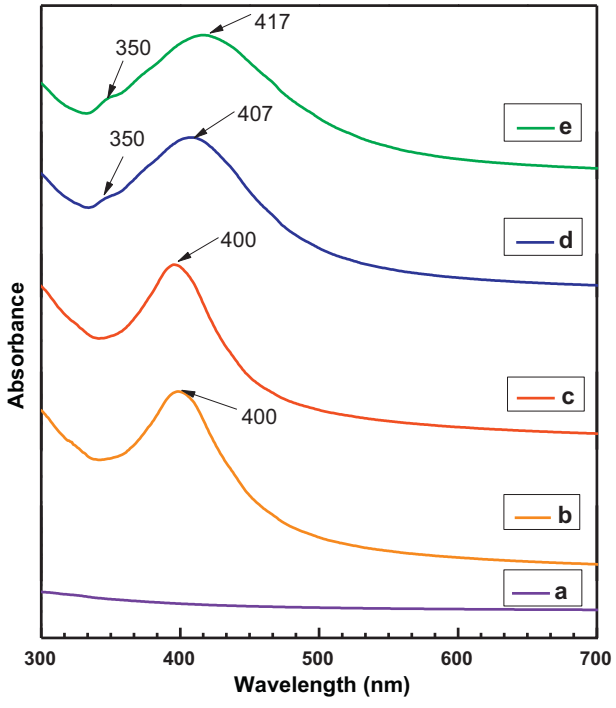

Fig. 1. UV–Visible absorption spectra of the Ag nanoparticle-GrO suspension in aqueous medium. (a) GrO, (b) 1×10^{-3} mol dm^{-3} $AgNO_3$, (c) 2×10^{-3} mol dm^{-3} $AgNO_3$, (d) 4×10^{-3} mol dm^{-3} $AgNO_3$, and (e) 8×10^{-3} mol dm^{-3} $AgNO_3$.

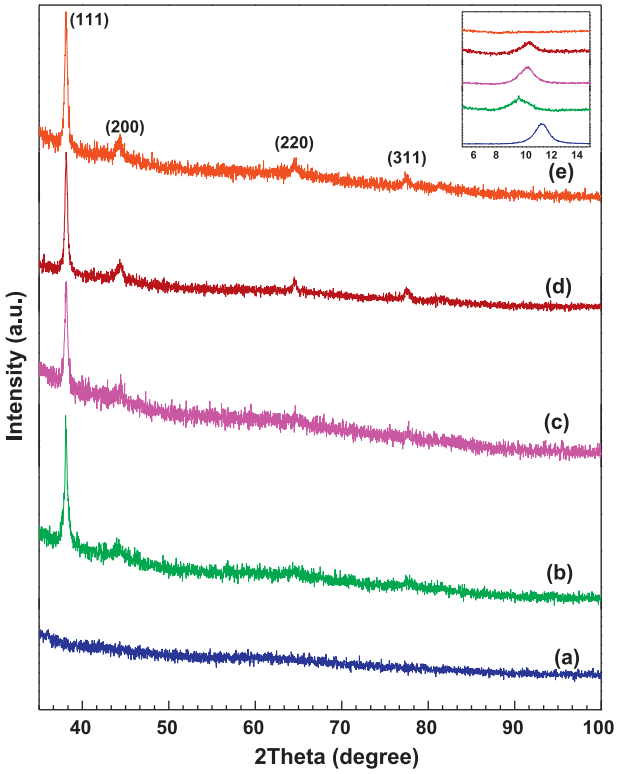

Fig. 2. XRD of the synthesized Ag nanoparticles using different concentration of the $AgNO_3$ solution (a) GrO, (b) 1×10^{-3} mol dm^{-3} $AgNO_3$, (c) 2×10^{-3} mol dm^{-3} $AgNO_3$, (d) 4×10^{-3} mol dm^{-3} $AgNO_3$, and (e) 8×10^{-3} mol dm^{-3} $AgNO_3$.

Table 1
FWHM, crystallite size and lattice constant are calculated from XRD of synthesized Ag nanoparticles.

Parameters	1×10^{-3} mol dm^{-3} $AgNO_3$	2×10^{-3} mol dm^{-3} $AgNO_3$	4×10^{-3} mol dm^{-3} $AgNO_3$	8×10^{-3} mol dm^{-3} $AgNO_3$
FWHM (degree)	0.71	0.383	0.323	0.333
Crystallite size (nm)	12	23	27	26
Lattice constant '*a*' (Å)	4.0880	4.0830	4.0862	4.0890

was used. XRD results confirm the formation of the Ag nanoparticles on the GrO matrix.

TEM images of Ag nanoparticles (Fig. 3) show the wide distribution of particles ranging in the diameter of 5–25 nm. Fig. 3(a) shows that the smaller particles are spherical in shape where as the larger nanoparticles are in an elongated form. The elongated shape could be the result of the aggregation of the two or more particles together (Fig. 3(b)–(d)). The size and shape of the Ag nanoparticles are also influenced by the concentration of $AgNO_3$ solution. Most of the nanoparticles are spherical in shape when synthesized using 1×10^{-3} mol dm^{-3} of $AgNO_3$ solution. As observed in Fig. 3(c) and (d), the synthesis of the Ag nanoparticles using higher concen-

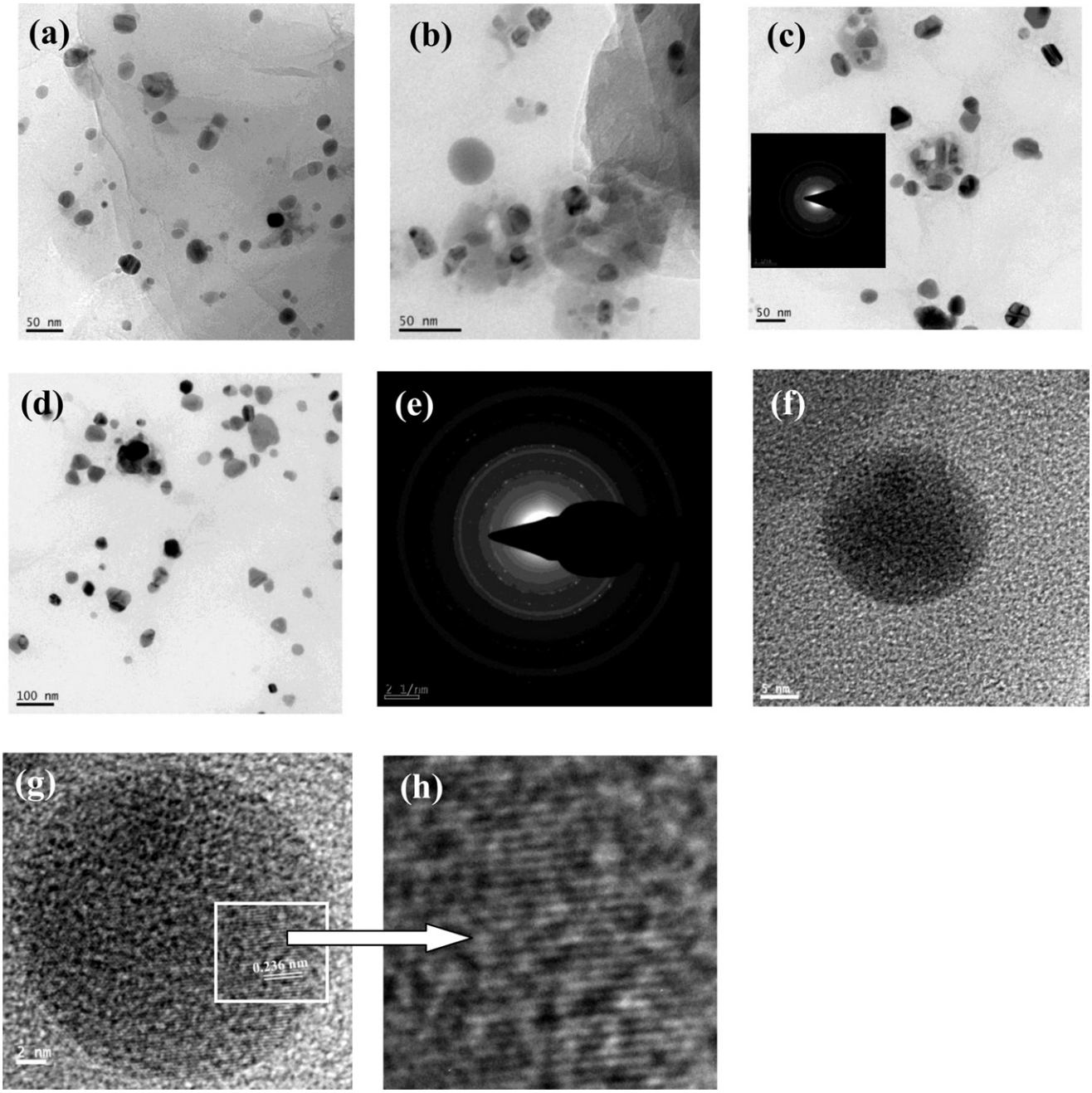

Fig. 3. TEM images of Ag nanoparticles on the GrO sheets (a) Ag nanoparticles synthesized at 1×10^{-3} mol dm^{-3} $AgNO_3$, (b) Ag nanoparticles synthesized at 2×10^{-3} mol dm^{-3} $AgNO_3$, (c) Ag nanoparticles synthesized at 8×10^{-3} mol dm^{-3} $AgNO_3$, inset: corresponding SAED image, (d) Ag nanoparticles synthesized at 8×10^{-3} mol dm^{-3} $AgNO_3$, (e) SAED image of the Ag nanoparticles synthesized using 1×10^{-3} mol dm^{-3} concentration of $AgNO_3$, (f) HRTEM images of the Ag nanoparticles synthesized at 1×10^{-3} mol dm^{-3} $AgNO_3$, (g) HRTEM with fringe spacing, and (h) enlarge image of fringe spacing.

tration of Ag salt (8×10^{-3} mol dm^{-3}) produces variable particle shapes. At this concentration nanoparticle with different shapes such as spherical, triangular, pentagonal, ellipsoid and rod are obtained. Nanoparticles are seen to be agglomerating when concentration of $AgNO_3$ solution used is higher than 2×10^{-3} mol dm^{-3} resulting in formation of bigger particles. Fig. 3(c) and (e) shows selected area electron diffraction (SAED) patterns of synthesized Ag nanoparticles with concentration of $AgNO_3$ as 8×10^{-3} mol dm^{-3} and 1×10^{-3} mol dm^{-3}, respectively. It indicates the crystalline nature of the Ag nanoparticles. The diffraction dots are resolved in the SAED images, implying the crystalline nature of the Ag nanoparticles. The HRTEM images of Ag nanoparticle embedded on the GrO sheets are shown in Fig. 3(f) and (g). TEM image of the transparent silk waves of the GrO sheets indicates that the Ag nanoparticles are deposited on the GrO support. The crystal lattice of Ag nanoparticles as well as fringes of GrO are resolved at few regions. The measured fringe lattice of Ag nanoparticles is found to be 0.236 nm which corresponds to the (1 1 1) crystal plane (Fig. 3(g) and (h)) [15].

There are few reports on the Ag nanoparticles decorated on the GrO sheets. Recently Shen et al. reported the solution based synthesis of Ag nanoparticles in CCG using mixed reducing agent and found the homogeneous distribution of Ag nanoparticles of size range 5–10 nm on CCG [23]. The average crystallite size of the Ag nanoparticles from the (1 1 1), (2 0 0) and (2 2 0) XRD crystallographic plane based on Sherrer's equation was 8 nm which is also supported by the TEM analysis. Pasricha et al. also reported the solution-based synthesis of Ag nanoparticles into the GrO sheets without using any reducing agent [15]. In this report it is confirmed by TEM analysis that the Ag nanoparticles of size ranged 3–12 nm were decorated on to the GrO sheets. Formation of bigger particle due to agglomeration of the smaller particles was also observed. Lu et al. reported a novel synthesis method for the decoration of aerosol Ag nanocrystals on the GrO sheet [13]. The aerosol Ag nanocrystals were synthesized using a mini-arc plasma reactor and subsequent deposition of as-synthesized nanocrystals onto a GrO. HRTEM analysis conformed that the Ag nanocrystals of about 5–10 nm were attached to the GrO sheet. Zhou et al. also reported the single step *in situ* synthesis of Ag nanoparticles on single layer GrO or reduced GrO surfaces under thermal condition without any surfactant or reducing agent [12]. This method resulted Ag nanoparticles in the size range of few nanometers to 1 μm with non uniform size. Whereas the Ag nanoparticles, obtained by using solution phase synthesis, the method reported in this study, are about 5–25 nm in size with variable shape. It is also observed that the shape of the nanoparticle is dependent on concentration of $AgNO_3$ solution.

The bactericidal test was performed against two Gram negative bacteria, *E. coli* and *P. aeruginosa* on nutrient agar plates containing 60 μL of different Ag nanoparticle–GrO hybrids. It was observed that both the bacterial strains were sensitive to synthesized Ag nanoparticles by using different concentrations of $AgNO_3$ (1×10^{-3} mol dm^{-3} (AgNP1), 2×10^{-3} mol dm^{-3} (AgNP2), 4×10^{-3} mol dm^{-3} (AgNP3), 8×10^{-3} mol dm^{-3} (AgNP4)) and recorded zone of inhibitions from 7 to 26 mm (Fig. 4). It was also observed that *P. aeruginosa* was comparatively more sensitive to the Ag nanoparticles and produced maximum growth inhibition zone (26 ± 1.53 mm, $n = 3$, n = numbers of experimental results) of AgNP4 followed by inhibition zone of AgNP3 (23 ± 1 mm, $n = 3$), AgNP2 (19 ± 1.53 mm, $n = 3$) and AgNP1 (16 ± 1.15 mm, $n = 3$) suspension (Fig. 4). However, *E. coli* exhibited maximum growth inhibition of AgNP4 (18 ± 0.58 mm, $n = 3$) followed by AgNP3 (13 ± 1 mm, $n = 3$), AgNP2 (10 ± 1.53 mm, $n = 3$) and AgNP1 (7 ± 1 mm, $n = 3$) suspension (Fig. 4). The zone inhibition of *E. coli* and *P. aeruginosa* with different Ag nanoparticles are depicted in Fig. 5. It shows that the variation in concentration of $AgNO_3$ used for the synthesis of Ag nanoparticles affects bacterial growth. Shen et al. investigated the antibacterial activity of Ag-CCG composite against *Colibacillus*, *Staphylococcus aureus* and *Canidia albicans* bacteria [23]. However, the detailed investigation on the antibacterial activity of this hybrid material is not reported.

The bacterial growth kinetics is monitored in 10 mL nutrient broth supplemented with synthesized Ag nanoparticles at different conditions. It showed that the nanoparticles prepared using different concentration of $AgNO_3$ caused a growth delay of *P. aeruginosa* and *E. coli*. The growth delay follows the order as AgNP1 < AgNP2 < AgNP3 < AgNP4 (Fig. 6a and b). Increasing the concentration of the nanoparticles increases the growth delay of *P. aeruginosa* and *E.coli*, indicates that the concentration of the Ag nanoparticles is a prime parameter for the antibacterial activity. Recently Pal et al. reported the shape dependence of the antibacterial activity of Ag nanoparticles against *E. coli*, both in liquid system and agar plate [30]. There are some reports on the study of the antimicrobial effect of Ag nanoparticle immobilized on carbon based materials [50–52]. Carbon-based nanomaterials (CBNs) such as single walled carbon nanotubes (SWNTs), multiwalled carbon nanotubes (MWNTs), aqueous phase C60 nanopartilces (aq-nC60)

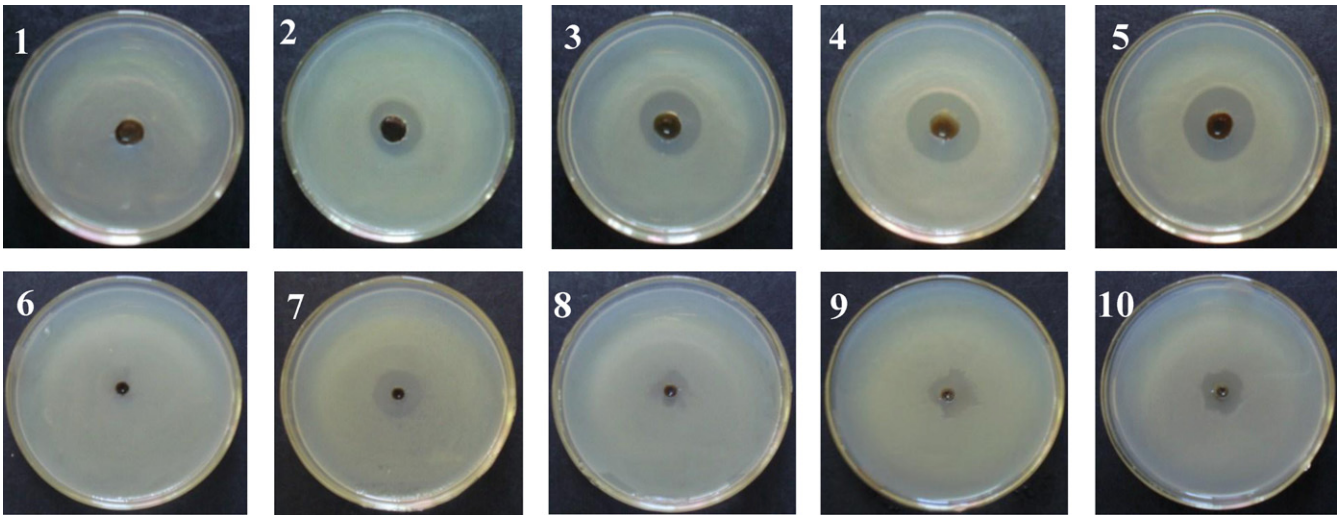

Fig. 4. Zone of inhibition produced by different concentrations of Ag nanoparticles with bacteria: 1, control (GrO); 2–5, zone of inhibition produced with *P. aeruginosa* by AgNP1, AgNP2, AgNP3 and AgNP4 of the suspension of nutrient agar of nanoparticles respectively; 6, control (GrO); 7–10, zone of inhibition produced with *E. coli* by AgNP1, AgNP2, AgNP3 and AgNP4 of the suspension in nutrient agar of nanoparticles respectively.

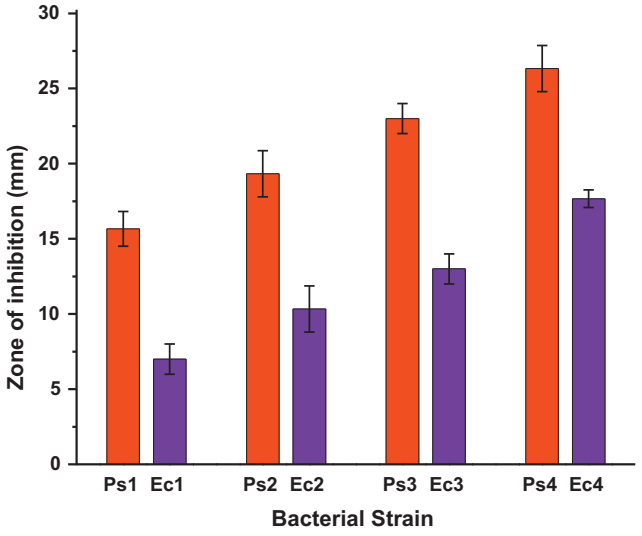

Fig. 5. Effect of Ag nanoparticles on growth of *P. aeruginosa* and *E. coli*; Ps: *P. aeruginosa*; Ec: *E. coli*. Ps1, Ps2, Ps3 and Ps4 stand for inhibition zone produced by *P. aeruginosa* with AgNP1, AgNP2, AgNP3 and AgNP4 per mL concentration of Ag nanoparticles, respectively; Ec1, Ec2, Ec3 and Ec4 stand for inhibition zone produced by *E. coli* with AgNP1, AgNP2, AgNP3 and AgNP4 per mL concentrations of Ag nanoparticles, respectively.

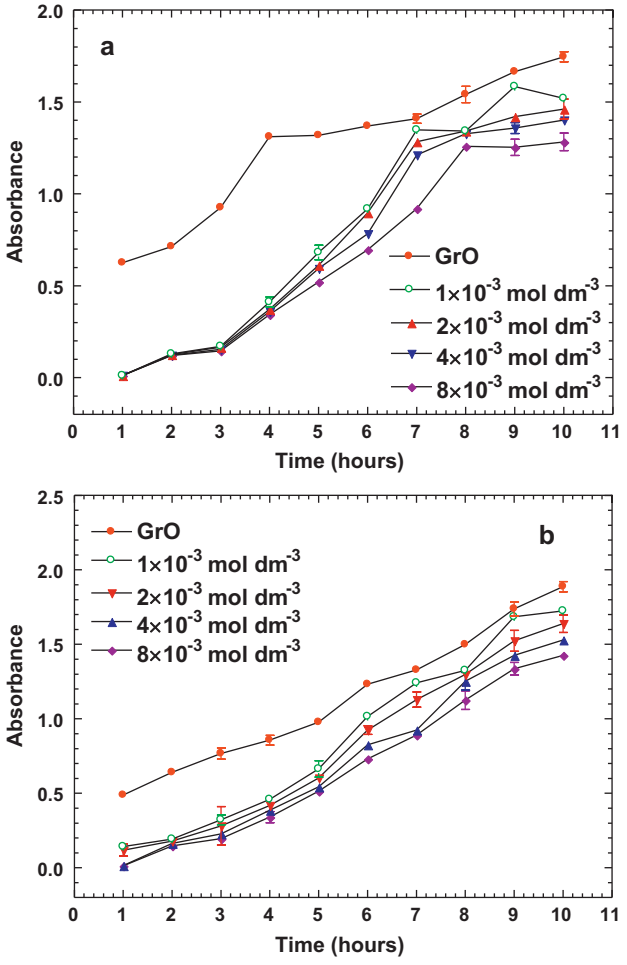

Fig. 6. Growth kinetics curve of (a) *P. aeruginosa* and (b) *E. coli* in NB.

and colloidal graphite induced bacterial cytotoxicity and SWNTs exhibited the highest cytotoxicity towards *E. coli*, *P. aeruginosa*, *Bacillus subtilis* and *Staphylococcus epidermis* [50]. They also studied the bacterial cytotoxicity of CBNs against Gram negative bacteria and Gram positive bacteria in presence of Suwannee River-natural organic matter (SR-NOM). The surface modification of nanomaterials by NOM reduces the deposition and attachment of bacteria on the surface of the nanomaterials. Similarly, Kang et al. reported that highly purified SWNTs exhibit strong antimicrobial activity and showed that *E. coli* has undergone severe membrane damage and subsequent lost of viability due to SWNTs [52]. Yaun et al. investigated the antimicrobial effect of functionalized MWNTs against *S. aureus*, *E. coli* and *P. aeruginosa* [51]. They found that dendrimer modified MWNTs and Ag nanoparticle immobilized MWNTs shows stronger antimicrobial effect than MWNTs against all three bacteria. In our study also graphene oxide alone does not show the antimicrobial effect against *E. coli* and *P. aeruginosa* barcteria. But Ag nanoparticle modified graphene oxide sheets show good antimicrobial properties. The mechanism of inhibitory action of Ag ions on microorganisms show that DNA loses its replication ability and expression of ribosomal subunit proteins as well as some other cellular proteins and enzymes due to Ag treatment [53]. It was also anticipated that a bacterial cell in contact with Ag nanoparticles takes in Ag ions, which inhibit a respiratory enzyme(s), facilitating the generation of reactive oxygen species and consequently damaging the cell.

4. Conclusions

We have demonstrated the synthesis of Ag nanoparticles in solution phase chemical reduction of $AgNO_3$ with $NaBH_4$ in presence of GrO suspension. The size and shape of the Ag nanoparticles are dependent on the concentration of Ag salt. The nanoparticle of different shape such as spherical, triangular, pentagonal, ellipsoid and rod are obtained at the higher concentration of the Ag salt (8×10^{-3} mol dm^{-3}). The synthesized Ag nanoparticles show good antimicrobial activity against the Gram negative bacteria *E. coli* and *P. aeruginosa* which is dependent on size and shape of Ag nanoparticles. The as-synthesized Ag nanoparticles can be useful for several applications in biological area as well as materials science.

Acknowledgements

The authors thank the Ministry of Mines, Govt. of India, New Delhi, for financial support and the Director, North East Institute of Science and Technology (NEIST), CSIR, Jorhat, India for the interest in this work and facilities. VSK and MVS acknowledge CSIR for financial support. Authors acknowledge Ms. Pooja Mudellu for providing AFM images.

Appendix A. Supplementary data

Supplementary data associated with this article can be found, in the online version, at doi:10.1016/j.colsurfb.2010.10.033.

References

[1] K.S. Novoselov, A.K. Geim, S.V. Morozov, D. Jiang, Y. Zhang, S.V. Dubonos, I.V. Grigorieva, A.A. Firsov, Science 306 (2004) 666.
[2] A.K. Geim, K.S. Novoselov, Nat. Mater. 6 (2007) 183.
[3] K.S. Novoselov, A.K. Geim, S.V. Morozov, D. Jiang, M.I. Katsnelson, I.V. Grigorieva, S.V. Dubonos, A.A. Firsov, Nature 438 (2005) 197.
[4] X. Li, X. Wang, L. Zhang, S. Lee, H. Dai, Science 319 (2008) 1229.
[5] S. Stankovich, D.A. Dikin, G.H.B. Dommett, K.M. Kohlhaas, E.J. Zinney, E.A. Stach, R.D. Piner, S.T. Nguyen, R.S. Ruoff, Nature 442 (2006) 282.
[6] F. Schedin, A.K. Geim, S.V. Morozov, E.W. Hill, P. Blake, M.I. Katsnelson, K. Novoselov, Nat. Mater. 6 (2007) 652.

[7] D. Li, M.B. Muller, S. Gilje, R.B. Kaner, G.G. Wallance, Nat. Nanotechnol. 3 (2008) 101.
[8] S. Park, R.S. Ruoff, Nat. Nanotechnol. 4 (2009) 217.
[9] Z.S. Pillai, P.V. Kamat, J. Phys. Chem. B 108 (2004) 945, and references therein.
[10] Y. Sun, Y. Xia, Science 298 (2002) 2176, and references therein.
[11] G. Hodes, Adv. Mater. 19 (2007) 639.
[12] X. Zhou, X. Huang, X. Qi, S. Wu, C. Xue, F.Y.C. Boey, Q. Yan, P. Chen, H. Zhang, J. Phys. Chem. C 113 (2009) 10842.
[13] G. Lu, S. Mao, S. Park, R.S. Ruoff, J. Chen, Nano Res. 2 (2009) 192.
[14] N. Severin, S. Kirstein, I.M. Sokolov, J.P. Rabe, Nano Lett. 9 (2009) 457.
[15] R. Pasricha, S. Gupta, A.K. Srivastava, Small 20 (2009) 2253.
[16] C. Xu, X. Wang, J.W. Zhu, X.J. Yang, L. Lu, J. Mater. Chem. 46 (2008) 5625.
[17] G. Williams, B. Seger, P.V. Kamat, ACS Nano 2 (2008) 1487.
[18] R. Muszynski, B. Seger, P.V. Kamat, J. Phys. Chem. C 112 (2008) 5263.
[19] I.V. Ligtcap, T.H. Kosel, P.V. Kamat, Nano Lett. 10 (2010) 577.
[20] G.M. Scheuermann, L. Rumi, P. Steurer, W. Bannwarth, R. Mulhaupt, J. Am. Chem. Soc. 131 (2009) 8262.
[21] B.-S. Kong, J. Geng, H.-T. Jung, Chem. Commun. 16 (2009) 2174.
[22] C. Xu, X. Wang, J. Zhu, J. Phys. Chem. C 112 (2008) 19841.
[23] J. Shen, M. Shi, N. Li, H. Ma, M. Ye, Nano Res. 3 (2010) 339.
[24] J. Shen, Y. Hu, M. Shi, N. Li, H. Ma, M. Ye, J. Phys. Chem. C 114 (2010) 1498.
[25] W. Hu, C. Peng, W. Luo, M. Lv, X. Li, D. Li, Q. Huang, C. Fan, ACS Nano 7 (2010) 4317.
[26] O. Akhavan, E. Ghaderi, J. Phys. Chem. C 113 (2009) 20214.
[27] A. Frattini, N. Pellegri, D. Nicastro, O. de Sanctis, Mater. Chem. Phys. 94 (2005) 148.
[28] P. Li, J. Li, C. Wu, Q. Wu, J. Li, J. Nanotechnol. 16 (2005) 1912.
[29] I. Sondi, B. Salopek-Sondi, J. Colloid Interface Sci. 275 (2004) 177, and references therein.
[30] S. Pal, Y.K. Tak, J.M. Song, Appl. Environ. Microbiol. 73 (2007) 1712, and references therein.
[31] V.K. Sharma, R.A. Yngard, Y. Lin, Adv. Colloid Interface Sci. 145 (2009) 83.
[32] R.W.-Y. Sun, R. Chen, N.P.-Y. Chung, C.-M. Ho, C.-L.S. Lin, C.-M. Che, Chem. Commun. 40 (2005) 5059.
[33] V. Alt, T. Bechert, P. Steinrücke, M. Wagener, P. Seidel, E. Dingeldein, Biomaterials 25 (2004) 4383.
[34] H.Y. Lee, H.K. Park, Y.M. Lee, K. Kim, S.B. Park, Chem. Commun. 28 (2007) 2959.
[35] A.D. Russell, W.B. Hugo, Prog. Med. Chem. 31 (1994) 351.
[36] C. Aymonier, U. Schlotterbeck, L. Antonietti, P. Zacharias, R. Thomann, J.C. Tiller, S. Mecking, Chem. Commun. 24 (2002) 3018.
[37] A. Kumar, P.K. Vemula, P.M. Ajayan, G. John, Nat. Mater. 7 (2008) 236.
[38] H. Lepape, F. Solano-Serena, P. Contini, C. Devillers, A. Maftah, P. Leprat, Carbon 40 (2002) 2947.
[39] H. Lepape, F. Solano-Serena, P. Contini, C. Devillers, A. Maftah, P. Leprat, J. Inorg. Biochem. 98 (2004) 1054.
[40] H. Ortiz-Ibarra, N. Casillas, V. Soto, M. Barcena-Soto, R. Torres-Vitela, W. de la Cruz, S. Gómez-Salazar, J. Colloid Interface Sci. 314 (2007) 562.
[41] K.I. Yoon, J.H. Byeon, C.W. Park, J. Hwang, Environ. Sci. Technol. 42 (2008) 1251.
[42] R. Bhattacharya, P. Mukherjee, Adv. Drug. Deliv. Rev. 60 (2008) 1289.
[43] W.S. Hummers, R.E. Offeman, J. Am. Chem. Soc. 80 (1958) 1339.
[44] U. Schillinger, F.K. Lücke, Appl. Environ. Microbiol. 55 (1989) 1901.
[45] F. Douglas, R. Yañez, J. Ros, J. Marín, A. De la. Escosura-Muñiz, S. Alegret, A. Merkoçi, J. Nanopart. Res. 10 (2008) 97.
[46] P. Sarkar, D.K. Bhui, H. Bar, G.P. Sahoo, S.P. De, A. Misra, J. Luminescence 129 (2009) 704.
[47] A.S. Reddy, C.-Y. Chen, S.C. Bakerb, C.-C. Chen, J.-H. Jean, C.-W. Fan, H.-R. Chen, J.-C. Wang, Mater. Lett. 63 (2009) 1227.
[48] U. Kreibig, M. Voltmer, Optical Properties of Metal Clusters, 25, Springer, Berlin, Germany, 1995.
[49] P. Mulvaney, Langmuir 12 (1996) 788.
[50] S. Kang, M.S. Mauter, M. Elimelech, Environ. Sci. Technol. 43 (2009) 2648.
[51] W. Yaun, G. Jiang, J. Che, X. Qi, R. Xu, M.W. Chang, Y. Chen, S.Y. Lim, J. Dai, M.B. Chan-Park, J. Phys. Chem. C 112 (2008) 18754.
[52] S. Kang, M. Pinault, L.D. Pfefferle, M. Elimelech, Langmuir 23 (2007) 8670.
[53] Q.L. Feng, J. Wu, G.Q. Chen, F.Z. Cui, T.M. Kim, J.O. Kim, J. Biomed. Mater. Res. 52 (2000) 662.